

Probing photodissociation dynamics using ring polymer molecular dynamics

Cite as: J. Chem. Phys. **150**, 114105 (2019); <https://doi.org/10.1063/1.5086218>

Submitted: 19 December 2018 . Accepted: 27 February 2019 . Published Online: 18 March 2019

Rajwant Kaur, and Ralph Welsch 



View Online



Export Citation



CrossMark



Probing photodissociation dynamics using ring polymer molecular dynamics

Cite as: J. Chem. Phys. 150, 114105 (2019); doi: 10.1063/1.5086218

Submitted: 19 December 2018 • Accepted: 27 February 2019 •

Published Online: 18 March 2019



Rajwant Kaur and Ralph Welsch^{a)} 

AFFILIATIONS

Center for Free-Electron Laser Science, DESY, Notkestrasse 85, 22607 Hamburg, Germany

^{a)}Electronic mail: ralph.welsch@desy.de

ABSTRACT

The performance of the ring polymer molecular dynamics (RPMD) approach to simulate typical photodissociation processes is assessed. The correct description of photodissociation requires the calculation of correlation functions or expectation values associated with non-equilibrium initial conditions, which was shown to be possible with RPMD very recently [J. Chem. Phys. **145**, 204118 (2016)]. This approach is combined with treatment of the nonadiabatic dynamics employing the ring polymer surface hopping approach (RPSH), which is based on Tully's fewest switches surface hopping (FSSH) approach. The performance is tested using one-dimensional photodissociation models. It is found that RPSH with non-equilibrium initial conditions can well reproduce the time-dependent dissociation probability, and adiabatic and diabatic populations for cases where the crossing point is below and above the Franck-Condon point, respectively, while standard FSSH fails to reproduce the exact quantum dynamics in the latter case. Thus, it is shown that RPSH is an efficient and accurate alternative to standard FSSH, which is one of the most widely employed approaches to study photochemistry.

Published under license by AIP Publishing. <https://doi.org/10.1063/1.5086218>

I. INTRODUCTION

Photochemical processes are ubiquitous in nature, and the dynamics of these processes is important in chemical and biological reactions such as isomerization reactions, e.g., in the retinal protein rhodopsin,^{1,2} photo-deactivation pathways for nucleobases,^{3–6} charge transfer reactions in materials,^{7–11} material designs for renewable energy harvesting,¹² photoinduced surface reactions,¹³ and proton-coupled electron transfer.^{14–16} In these processes, the Born-Oppenheimer approximation typically breaks down and therefore, nuclear and electronic motions are coupled. Exact quantum dynamical methods, e.g., the multiconfigurational time-dependent Hartree approach (MCTDH),^{17–19} can readily simulate the coupled motions of nuclei and electrons. However, exact quantum dynamics simulations for coupled systems are limited to model systems or systems with only a few degrees of freedom due to the high numerical cost of the calculations.^{20–25} Therefore, approximate methods are often used to study photochemical processes in larger systems. Among the most used approximate schemes are mixed quantum-classical approaches such as Tully's fewest switches surface hopping (FSSH)^{26–28} or the *ab initio*

multiple spawning approach.²⁹ However, these approaches treat the nuclei classically and thus ignore nuclear quantum effects (NQE) such as zero-point energy and tunneling, which are, in particular, important for cases when light nuclei are involved in the dynamics.

Various methods have emerged that approximately include NQE in classical-like simulations of thermal processes in the ground electronic state. Among the most used ones is the ring polymer molecular dynamics (RPMD) approach.^{30–35} RPMD is based on the imaginary-time path-integral formalism that maps a quantum Boltzmann distribution onto a set of classical replicas in phase space joined by harmonic springs, which is known as a ring polymer. Within RPMD, dynamical quantities like real-time correlation functions are obtained by classical dynamics in this extended ring polymer phase space. However, the original formulation of RPMD does not allow for the simulation of photochemical processes as it is restricted to the thermal process on a single adiabatic potential energy surface (PES). Recently, it was shown that RPMD can be effectively used to calculate correlation functions and expectation values associated with non-equilibrium initial conditions, e.g., following photoexcitation.³⁶ The RPMD approach

with non-equilibrium initial conditions can be obtained from Matsubara dynamics³⁷ in a similar manner as the original RPMD approach³⁸ and thus inherits the same well-known properties, e.g., it is exact in the high-temperature and classical limits, for dynamics in harmonic potentials and it conserves the average energy of the springs.³⁶ Numerical tests³⁶ showed very similar behavior of RPMD when calculating properties associated with equilibrium and non-equilibrium initial conditions, respectively. Therefore, it is expected that RPMD gives similar accuracy for calculations with equilibrium and non-equilibrium initial conditions, and thus, it fails to describe cases where, e.g., real-time coherences are important or when certain specific vibrational modes are extracted.^{39,40} Yet calculations in Ref. 36 were limited to dynamics on a single PES.

Several modifications to the original RPMD approach to investigate nonadiabatic dynamics have been proposed.^{41–48} These extensions make use of the Meyer-Miller-Stock-Thoss representation,^{41–44} FSSH,^{45–47} or the position representation of RPMD.⁴⁸ Ideally, any nonadiabatic version of RPMD would exhibit the following features: preserving the quantum Boltzmann distribution and capturing the correct electron dynamics, e.g., capturing Rabi oscillations in a two-level system.⁴⁹ Unfortunately, none of the nonadiabatic RPMD approaches available satisfies all these conditions. While mapping-variable (MV) RPMD⁴² and kinetically constrained (KC) RPMD⁴⁸ preserve the quantum Boltzmann distribution although it is approximate for KC-RPMD, they do not capture Rabi oscillations. Nonadiabatic (N) RPMD⁴¹ and coherent-state (CS) RPMD⁴⁴ can both capture Rabi oscillations but do not conserve the quantum Boltzmann distribution. Ring polymer surface hopping (RPSH)⁴⁵ provides an accurate and explicit description of the electronic dynamics but again does not conserve the quantum Boltzmann distribution. It should be pointed out that the problems with conserving the quantum Boltzmann distribution in RPSH are inherited from the underlying FSSH approach. FSSH does not satisfy detailed balance due to the time-irreversibility and overcoherence problem in the surface hopping part. This is a well known and well studied problem in FSSH. There exist methods that can alleviate this problem and that approximately satisfy detailed balance.^{50–53}

One of the most challenging and also intriguing regimes in photochemistry is the nonadiabatic tunneling regime, which has attracted attention recently.⁵⁴ In this regime, the energy of the excited molecule is not high enough to traverse the conical intersection (CI) or avoided crossing that lead to the dissociative state, classically, and thus the photodissociation is initiated by tunneling. This regime cannot be described with classical FSSH due to the lag of nuclear quantum effects, and exact quantum dynamics approaches are often too expensive.⁵⁴ In this article, we investigate the prospects of RPMD to describe photochemical processes, in particular, in the nonadiabatic tunneling regime, associated with non-equilibrium initial conditions and occurring on multiple coupled PESs. To this end, we will employ RPSH to describe the nonadiabatic dynamics. The manuscript is organized as follows: Sec. II describes briefly the methods employed. Section III gives the numerical parameters used in this work, and Sec. IV discusses the results for a one-dimensional photodissociation potential, followed by conclusions in Sec. V.

II. METHODS

A. Ring polymer molecular dynamics

RPMD approximates the Kubo transformed quantum real-time correlation function⁵⁵

$$\tilde{C}_{AB}(t) = \frac{1}{Z\beta} \int_0^\beta d\lambda \text{Tr}[e^{-\lambda\hat{H}} \hat{A} e^{-(\beta-\lambda)\hat{H}} e^{\frac{i\hat{H}t}{\hbar}} \hat{B} e^{-\frac{i\hat{H}t}{\hbar}}], \quad (1)$$

where $\beta = 1/k_B T$ and $\hat{H} = \hat{p}^2/2m + V(\hat{q})$ is the Hamiltonian for a one-dimensional system with $Z = \text{Tr}[e^{-\beta\hat{H}}]$, as the quantum mechanical partition function. In the following, equations are given for one-dimensional systems, but they are easily generalized to multiple dimensions. The RPMD approximation to Eq. (1) is given as³⁰

$$\tilde{C}_{AB}(t) = \frac{1}{Z_n(2\pi\hbar)^n} \int d\mathbf{p}_0 \int d\mathbf{q}_0 e^{-\beta_n H_n(\mathbf{p}_0, \mathbf{q}_0)} A(\mathbf{p}_0, \mathbf{q}_0) B(\mathbf{p}_t, \mathbf{q}_t), \quad (2)$$

where $\beta_n = \beta/n$ and the ring polymer Hamiltonian H_n is given as³⁰

$$H_n(\mathbf{p}, \mathbf{q}) = \sum_{j=1}^n \frac{p_j^2}{2m} + U_n(\mathbf{q}), \quad (3)$$

and the ring polymer potential is given as

$$U_n(\mathbf{q}) = \sum_{j=1}^n \left[\frac{m}{2} \omega_n^2 (q_j - q_{j+1})^2 + V(q_j) \right], \quad (4)$$

with $\omega_n = \frac{1}{\beta_n \hbar}$ and $q_{n+1} = q_1$. The partition function for the fictitious ring polymer is

$$Z_n = \frac{1}{(2\pi\hbar)^n} \int d\mathbf{p}_0 \int d\mathbf{q}_0 e^{-\beta_n H_n(\mathbf{p}_0, \mathbf{q}_0)}. \quad (5)$$

The operators \hat{A} and \hat{B} are functions of the position and momentum and are evaluated at the ring polymer coordinates as

$$A(\mathbf{p}, \mathbf{q}) = \frac{1}{n} \sum_{j=1}^n A(p_j, q_j). \quad (6)$$

The classical equations of motion associated with the Hamiltonian in Eq. (3) determine the time evolution of the ring polymer coordinates $(\mathbf{p}_t, \mathbf{q}_t)$ as

$$\dot{p}_j = -m\omega_n^2(2q_j - q_{j-1} - q_{j+1}) - \frac{\partial V(q_j)}{\partial q_j}, \quad (7)$$

$$\dot{q}_j = \frac{p_j}{m}. \quad (8)$$

The centroid position (\bar{q}) and momentum (\bar{p}) of the ring polymer are given as

$$\bar{q} = \frac{1}{n} \sum_{j=1}^n q_j, \quad (9)$$

$$\bar{p} = \frac{1}{n} \sum_{j=1}^n p_j. \quad (10)$$

To describe photodissociation processes with RPMD, the original RPMD approach has to be extended in two ways. First, the non-equilibrium nature of the photo-excitation has to be accounted

for. Second, non-Born-Oppenheimer effects have to be accounted for to describe the dynamics in the excited states. In Secs. II B and II C, these extensions will be discussed.

B. Non-equilibrium initial conditions within RPMD

Very recently it was shown that RPMD can be used to approximate non-equilibrium time correlation functions and expectation values of the form³⁶

$$\tilde{C}_{AB}(t) = \frac{1}{Z\beta} \int_0^\beta d\lambda \text{Tr}[e^{-\lambda\hat{H}^{(0)}} \hat{A} e^{-(\beta-\lambda)\hat{H}^{(0)}} e^{\frac{i\hat{H}^{(1)}t}{\hbar}} \hat{B} e^{-\frac{i\hat{H}^{(1)}t}{\hbar}}], \quad (11)$$

$$\langle B \rangle(t) = \frac{1}{Z} \text{Tr}[e^{-\beta\hat{H}^{(0)}} e^{\frac{i\hat{H}^{(1)}t}{\hbar}} \hat{B} e^{-\frac{i\hat{H}^{(1)}t}{\hbar}}]. \quad (12)$$

Here, we will consider cases for which the two Hamiltonians, $\hat{H}^{(0)}$ and $\hat{H}^{(1)}$, differ only in the potential energy. For $i = 0, 1$,

$$\hat{H}^{(i)} = \frac{\hat{p}^2}{2m} + V^{(i)}(\hat{q}), \quad (13)$$

with $V^{(0)} \neq V^{(1)}$. The corresponding ring polymer Hamiltonians are³⁶

$$H_n^{(i)}(\mathbf{p}, \mathbf{q}) = \sum_{j=1}^n \frac{p_j^2}{2m} + U_n^{(i)}(\mathbf{q}), \quad (14)$$

$$U_n^{(i)}(\mathbf{q}) = \sum_{j=1}^n \left[\frac{m}{2} \omega_n^2 (q_j - q_{j+1})^2 + V^{(i)}(q_j) \right], \quad (15)$$

and the RPMD approximations to Eqs. (11) and (12) read³⁶

$$\tilde{C}_{AB}(t) = \frac{1}{Z_n(2\pi\hbar)^n} \int d\mathbf{p}_0 \int d\mathbf{q}_0 e^{-\beta_n H_n^{(0)}(\mathbf{p}_0, \mathbf{q}_0)} A(\mathbf{p}_0, \mathbf{q}_0) B(\mathbf{p}_t, \mathbf{q}_t), \quad (16)$$

$$\langle B \rangle(t) = \frac{1}{Z_n(2\pi\hbar)^n} \int d\mathbf{p}_0 \int d\mathbf{q}_0 e^{-\beta_n H_n^{(0)}(\mathbf{p}_0, \mathbf{q}_0)} B(\mathbf{p}_t, \mathbf{q}_t). \quad (17)$$

The time evolution of the ring polymer coordinates is calculated from $H_n^{(1)}$.³⁶

C. Ring polymer surface hopping

Several ways have been proposed to describe nonadiabatic effects in RPMD.^{41–48,56} In this work, we will use an extension which is based on FSSH.⁴⁵ We will briefly review FSSH first and then discuss the combination of RPMD with FSSH. The basic concept behind FSSH is the propagation of nuclei along classical trajectories, $R(t)$,²⁶ on a single adiabatic potential and the statistical switching to another adiabatic potential. The time-dependent electronic coefficients, $c_k(t)$, associated with each adiabatic state are obtained by solving the time-dependent Schrödinger equation in the adiabatic basis at the given trajectory, $R(t)$,

$$i\hbar\dot{c}_k = \sum_j c_j (V_{kj} - i\hbar\dot{R} \cdot d_{kj}), \quad (18)$$

where d_{jk} are the nonadiabatic coupling matrix elements and V_{kj} are the electronic Hamiltonian matrix elements. FSSH results depend on

the choice of the representation. It has been shown that the adiabatic representation provides better results than the diabatic representation.⁵⁷ We therefore employ an adiabatic basis and $V_{kj} = 0$ for $k \neq j$. The hopping probability for a single classical nuclear trajectory, $R(t)$, between the surfaces j and k is given as

$$g_{kj} = \frac{b_{jk}}{a_{kk}} \Delta t, \quad (19)$$

where $b_{jk} = -2\text{Re}(a_{jk}^* \dot{R} \cdot d_{jk})$, $a_{jk} = c_j c_k^*$, and Δt is the time step. The obtained value of g_{kj} is then compared to a uniform random number, ξ , $0 < \xi < 1$, and hopping occurs if $g_{kj} > \xi$. To conserve the total energy of the system, the velocity is adjusted every time hopping occurs. The adjustment is performed in the direction of nonadiabatic coupling vector, d_{jk} . However, the hop fails if the velocity component is too small to compensate for the energy change. Our implementation closely follows Refs. 58 and 59.

The combination of RPMD and FSSH, termed RPSH,⁴⁵ follows the basic idea of FSSH but propagates a ring polymer trajectory, $\mathbf{q}(t)$, on a single adiabatic surface. The whole ring polymer is then switched statistically to other surfaces. In RPSH, Eq. (18) can be propagated on the centroid level, called centroid approximation (CA),⁴⁵

$$i\hbar\dot{c}_k = \sum_j c_j (V_{kj}(\bar{q}) - i\hbar\dot{\bar{q}} \cdot d_{kj}) \quad (20)$$

or on the bead level, called bead approximation (BA),⁴⁵

$$i\hbar\dot{c}_k = \sum_j c_j \left[\frac{1}{n} \sum_{l=1}^n V_{kj}(q_l) - i\hbar \frac{1}{n} \sum_{l=1}^n \dot{q}_l \cdot d_{kj} \right]. \quad (21)$$

During a transition, all the beads hop to the new adiabatic PES. The positions of all beads remain unchanged, while the velocities of the beads are adjusted along the direction of nonadiabatic coupling vector to conserve the total energy as⁴⁶

$$\dot{q} = \dot{q} - \frac{1}{a_{kj}} \left(b_{kj} \pm \sqrt{b_{kj}^2 + 2a_{kj}c_{kj}} \right) d_{kj}/m, \quad (22)$$

with $a_{kj} = d_{kj}^2/m$ and $b_{kj} = \dot{q}d_{kj}$. In the CA, the energy is conserved on the centroid level by setting $c_{kj} = V_k(\bar{q}) - V_j(\bar{q})$.⁴⁶ In the BA, both energy conservation on the centroid level as well as on the ring polymer level, by setting $c_{kj} = \frac{1}{n} \sum_j V_k(q_j) - V_j(q_j)$, are used.⁴⁶ As in standard FSSH, the hop is rejected if the velocity component is too small to compensate for the energy change.

III. NUMERICAL PARAMETERS

A. One-dimensional avoided crossing model potential

We employ model potentials that describe the photodissociation along a single coordinate associated with a proton mass. The parameters for the potentials detailed below are given in Tables I and II. The ground state potential, V_0 , is a Morse oscillator,

$$V_0(q) = E^{(0)} \left(1 - e^{-a^{(0)}(q - q_0^{(0)})} \right)^2 - b^{(0)}. \quad (23)$$

The parameters of the ground state are changed throughout the paper to model different non-equilibrium initial conditions (cf. Tables I and II). The first excited state is also a Morse oscillator,

TABLE I. Parameters used in the strongly coupled diabatic model potential. All values given in a.u.

	V_0		V_{11}		V_{22}		V_{12}
$E^{(0)}$	0.04556	$E^{(1)}$	0.02278	$E^{(2)}$	0.003417	$V^{(12)}$	0.008
$a^{(0)}$	1.94, 0.97	$a^{(1)}$	0.686	$a^{(2)}$	1.95	$a^{(12)}$	32.0
$q_0^{(0)}$	2.50, 1.70	$q_0^{(1)}$	2.0	$q_0^{(2)}$	3.16	$q_0^{(12)}$	3.16
$b^{(0)}$	0.04556	$b^{(1)}$	0.0	$b^{(2)}$	0.003417	...	

$$V_{11}(q) = E^{(1)} \left(1 - e^{-a^{(1)}(q-q_0^{(1)})} \right)^2 - b^{(1)}, \quad (24)$$

while the second excited states is a purely dissociative state,

$$V_{22}(q) = E^{(2)} e^{-a^{(2)}(q-q_0^{(2)})} + b^{(2)}. \quad (25)$$

The excited states form an avoided crossing with a Gaussian shaped coupling term

$$V_{12}(q) = V^{(12)} \left(e^{-a^{(12)}(q-q_0^{(12)})^2} \right). \quad (26)$$

A depiction of the diabatic model states is given in Figs. 1(a) and 1(b).

B. Simulation details

Initial distributions are obtained by running a long trajectory and periodically resampling the ring polymer momenta from the Maxwell-Boltzmann distribution. Converged results are obtained with $n = 64$ beads. A modified Velocity-Verlet scheme⁶⁰ is used to integrate the equations of motion using a time step of 0.1 fs, and 5×10^3 trajectories are used to converge each set of results. The initial temperature is chosen as 300 K. RPMD results are obtained for both the CA and BA.⁴⁵ In CA, the energy conservation is treated on the centroid level,⁴⁶ and for BA, the energy is conserved on the bead level.⁴⁶ For comparison, we also performed simulations with BA, but conserving the energy only on the centroid level, which is termed BA-c here and gave very similar results as for the BA approximation. FSSH results with classical sampling are obtained by setting $n = 1$. For comparison, we also calculate classical FSSH results sampled from a Wigner distribution of the harmonic approximation of the ground electronic state. Exact results are obtained employing the Heidelberg MCTDH package for convenience.⁶¹

TABLE II. Parameters used in the weakly coupled diabatic model potential. All values given in a.u.

	V_0		V_{11}		V_{22}		V_{12}
$E^{(0)}$	0.04556	$E^{(1)}$	0.09112	$E^{(2)}$	0.003417	$V^{(12)}$	0.0005
$a^{(0)}$	1.94, 0.97	$a^{(1)}$	1.157	$a^{(2)}$	0.7	$a^{(12)}$	2.0
$q_0^{(0)}$	2.50, 1.70	$q_0^{(1)}$	2.0	$q_0^{(2)}$	5.5	$q_0^{(12)}$	4.3
$b^{(0)}$	0.04556	$b^{(1)}$	0.0	$b^{(2)}$	0.0	...	

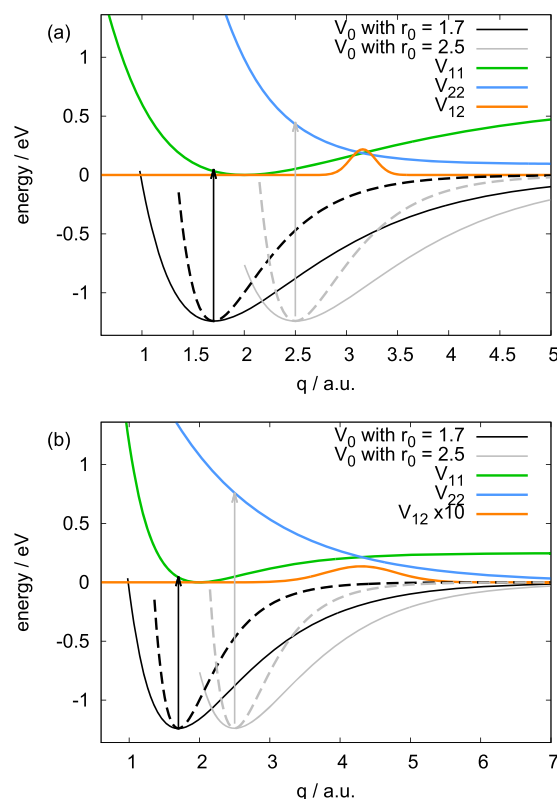


FIG. 1. Depiction of the diabatic models used in this work for the case of (a) strong and (b) weak coupling. The two excited diabatic states are given in green and blue, respectively. The diabatic coupling element is given in orange. Different ground electronic states exemplifying the different non-equilibrium initial conditions are given in black and gray. The black potentials have an equilibrium distance of $q_0^{(0)} = 1.7$ a.u., while the different line styles depict different initial frequencies. The gray potential has an equilibrium distance of $q_0^{(0)} = 2.50$ a.u. The initial excitation is depicted as arrows.

IV. RESULTS AND DISCUSSION

A. Dynamics with energetically low-lying avoided crossing

We start by considering excitation to the higher-lying state, which results in the crossing point in the strongly coupled diabatic model being 0.24 eV lower than the Franck-Condon point. This scenario is similar to scenarios previously studied with nonadiabatic RPMD variants^{43,46} but employs a particle with a much lower mass and therefore puts more emphasis on the nuclear quantum effects. The resulting nonadiabatic dynamics can, in general, be well described with FSSH. In Fig. 2, the time-dependent side-expectation value

$$\langle h \rangle(t) = \frac{1}{Z_n (2\pi\hbar)^n} \int d\mathbf{p}_0 \int d\mathbf{q}_0 e^{-\beta_n H_n^{(0)}(\mathbf{p}_0, \mathbf{q}_0)} h(\mathbf{q}_t), \quad (27)$$

where $h(\mathbf{q}_t) = \theta(\hat{q}_t - q_d)$ is a Heaviside function with respect to a dividing surface at $q_d = 6$ a.u., is given. This value measures

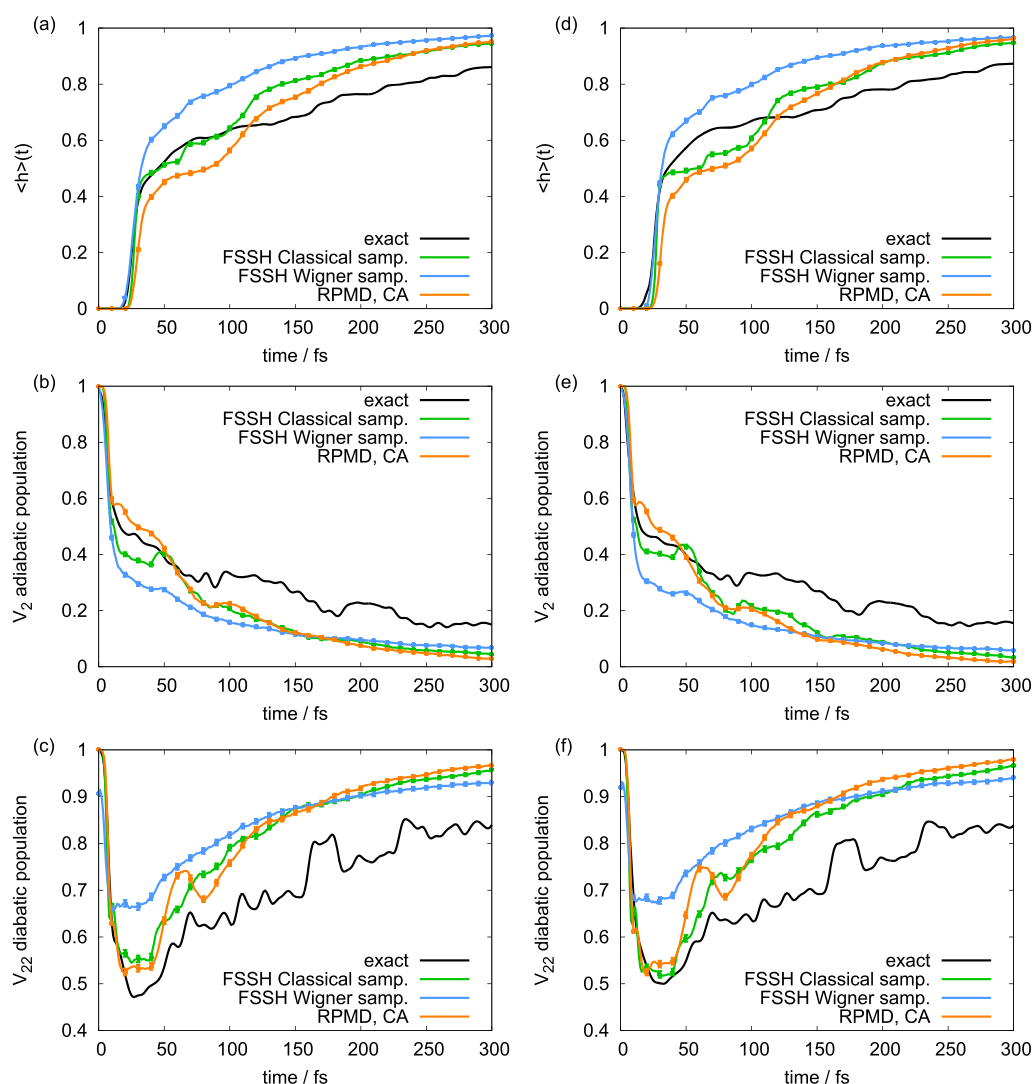


FIG. 2. Time-dependent side-expectation value [(a) and (d)], adiabatic [(b) and (e)], and diabatic populations [(c) and (f)] for two different initial vibrational frequencies of 1500 cm^{-1} [(a)–(c)] and 3000 cm^{-1} [(d) and (e)] employing the strong coupling model. The initial excitation is to the upper state. Exact results are given in black, FSSH results with classical sampling (i.e., $n = 1$) in green, FSSH results with Wigner sampling in blue, and RPMD results employing the CA are given in orange.

how much of our initial ensemble is dissociated, i.e., for which trajectory (or part of the wave packet) the coordinate value is larger than 6 a.u. Furthermore, Fig. 2 displays the adiabatic and diabatic populations of the upper adiabatic and diabatic potential, respectively. The dynamics is started from two different initial potentials with different initial frequencies, 1500 cm^{-1} and 3000 cm^{-1} . As can be expected for mostly downhill dynamics, there is little influence of the frequency of the initial potential on the population or the dissociation dynamics.

Overall the FSSH results with classical sampling ($n = 1$) and Wigner sampling perform well, and similar results are found for the RPMD simulations. Only RPMD results employing CA are shown as the results employing BA are similar. Yet, one can see that the longer-time behavior of the RPMD results compare better to the

exact results than the FSSH results. To exemplify the differences for the longer-time behavior, a linear fit to the side-expectation value between 100 fs and 300 fs is performed. The side-expectation value is expressed as $f(t) = \frac{1}{\tau}t + b$, and the dissociation time scale τ is extracted for each method (see Table III). While RPMD gives similar time scales as the exact approach, the often employed classical FSSH dynamics with Wigner sampling underestimates the dissociation time scale. Comparing dissociation time scales obtained employing the CA, BA, and BA-c, only small differences are seen.

For the case of the weakly coupled diabatic model, the crossing point is 0.54 eV lower than the Franck-Condon point. The resulting time-dependent side-expectation value shown in Fig. 3 for a initial vibrational frequency of 1500 cm^{-1} reaches unity within a few

TABLE III. Dissociation time scales τ in fs as fits of $f(t) = \frac{1}{\tau}t + b$ to the time-dependent side-expectation value $\langle h \rangle(t)$ between 100 and 300 fs for all different potentials and initial conditions considered in this paper. The different potentials are characterized by their coupling strength, initial equilibrium position (in a.u.), and initial vibrational frequency (in cm^{-1}). For the details on the method abbreviations, please see Sec. III B.

Method	Strong, 2.5		Strong, 1.7		Weak, 1.7
	1500	3000	1500	3000	1500
Exact	890	950	1 770	1 420	10 680
FSSH classical samp.	1130	910	121 700	176 430	...
FSSH Wigner samp.	1940	2140	7 430	5 500	8 430
RPMD, CA	790	820	2 480	2 530	18 570
RPMD, BA	1050	900	2 470	2 520	21 180
RPMD, BA-c	1070	1130	2 220	2 830	18 930

femtoseconds of the onset of dissociation. The side-expectation value and both the adiabatic and diabatic populations are well reproduced employing purely classical FSSH and RPMD using CA. However, both classical dynamics with Wigner sampling as well as RPMD with BA slightly overestimate the diabatic and slightly underestimate the adiabatic population displayed in Fig. 3, respectively.

B. Dynamics with energetically high-lying avoided crossing

The hardest to describe with classical dynamics are cases where the crossing point lies energetically higher than the Franck-Condon point and nonadiabatic tunneling is important for the dissociation. This is considered in the next example with excitation to the lower excited state close to the equilibrium position of V_{11} . With the equilibrium location of the ground state potential at 1.7 a.u., the avoided crossing is 0.15 eV and 0.17 eV above the Franck-Condon point for the strong and weak coupling model, respectively.

First, we will discuss the results for the strong coupling model shown in Fig. 4. Again, two different initial vibrational frequencies (1500 cm^{-1} and 3000 cm^{-1}) are considered. For this case, the initial conditions make more of a difference in the final results. The higher initial vibrational frequency results in an earlier onset of dissociation and an overall higher dissociation probability. The nonadiabatic dynamics for the strong coupling model and a Franck-Condon point below the avoided crossing is not reproduced by purely classical ($n = 1$) FSSH as it cannot capture the escape from the well at all. Including the zero point energy in the harmonic approximation employing Wigner sampling alleviates the problem, but in this case, FSSH tends to overestimate the dissociation probability due to the overestimation of the zero-point energy in the harmonic approximation. FSSH with Wigner sampling also has the onset of dissociation too early. The long time dissociation rate is strongly underestimated due to the purely classical dynamics. RPMD, on the other hand, matches the onset of dissociation very well, and also the long time dissociation rate is much better reproduced than in both FSSH variant. Again, only results for CA are shown as the

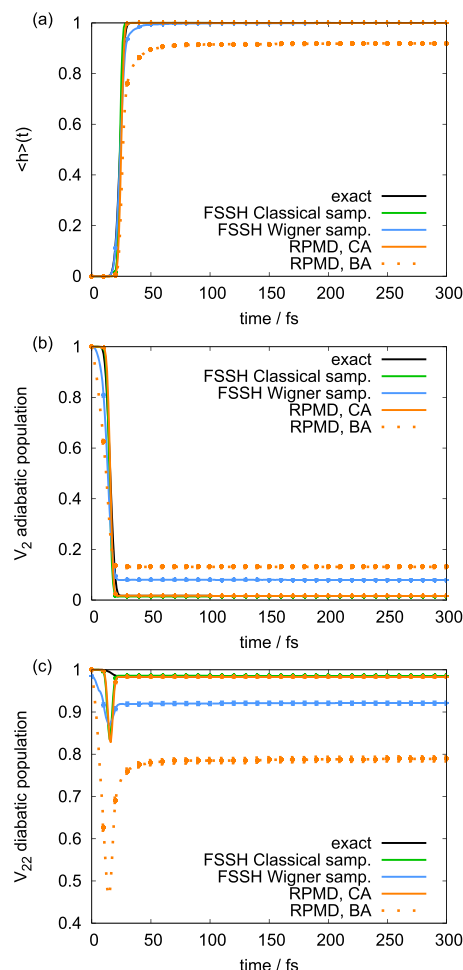


FIG. 3. Time-dependent side-expectation value (a), adiabatic (b), and diabatic populations (c) for an initial vibrational frequency of 1500 cm^{-1} employing the weak coupling model. The initial excitation is to the upper state. Exact results are given in black, FSSH results with classical sampling (i.e., $n = 1$) in green, FSSH results with Wigner sampling in blue, and RPMD results employing the CA are given in solid orange lines and employing the BA in dashed orange lines.

BA results are very similar. For the case of the lower initial vibrational frequency, the total dissociation probability is slightly overestimated by RPMD, while for the higher vibrational frequency, it is slightly underestimated. RPMD is capturing the diabatic populations well. However, the small, transient adiabatic population of the upper adiabatic state is not well reproduced for the strong coupling model.

The comparison of FSSH with classical and Wigner sampling shows the importance of zero-point energy effects in the photodissociation dynamics investigated here. Zero-point energy effects are exactly captured in RPMD including any anharmonic effects, while Wigner sampling, in practice, often, also in the current work, employs a harmonic approximation to the ground state potential energy surface. Therefore, the initial energy is overestimated and the extension of the initial position distribution is not reproduced

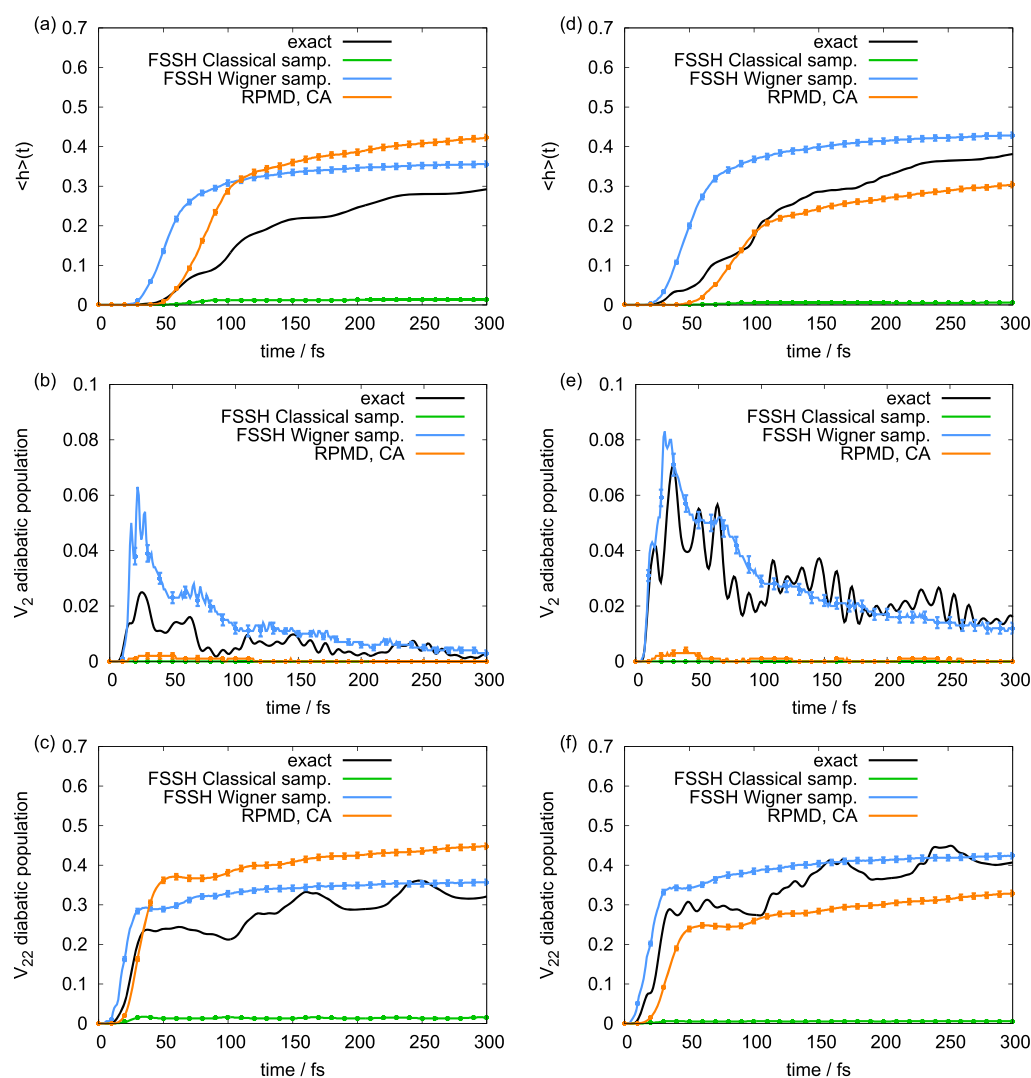


FIG. 4. Time-dependent side-expectation value [(a) and (d)], adiabatic [(b) and (e)], and diabatic populations [(c) and (f)] for two different initial vibrational frequencies of 1500 cm^{-1} [(a)–(c)] and 3000 cm^{-1} [(d) and (e)] employing the strong coupling model. The initial excitation is to the lower state. Exact results are given in black, FSSH results with classical sampling (i.e., $n = 1$) in green, FSSH results with Wigner sampling in blue, and RPMD results employing the CA are given in orange.

in Wigner sampling. In addition, zero-point energy is conserved throughout the RPMD dynamics, which is not the case for the classical FSSH trajectories employing Wigner sampling. While this is not a problem for the one-dimensional systems studied here, it can become problematic for higher-dimensional problems. Employing RPSH, therefore, will be a viable and efficient complement to FSSH for cases with highly anharmonic ground-state PES and high-dimensional problems showing zero-point energy leakage. The ability of RPMD to reproduce the longer-time dissociation time scale compared to both FSSH variants showcases the ability of RPMD to include tunneling effects in the dynamics.

The last example that will be considered here is the weak coupling model with an excitation such that the Franck-

Condon point is below the avoided crossing. The side-expectation value and adiabatic and diabatic populations are displayed in Fig. 5. Again, purely classical ($n = 1$) FSSH cannot capture the dissociation at all, while FSSH with Wigner sampling strongly overestimates the dissociation probability and underestimates the onset of dissociation due to the overestimation of the zero-point energy. For this case, FSSH with Wigner sampling also does not reproduce the diabatic or the adiabatic populations well. RPMD with CA or BA captures the whole dissociation, i.e., the onset of dissociation, the overall dissociation probability, as well as the long-time dissociation rate, very well. The adiabatic and diabatic populations are also well reproduced by RPMD but only if CA is employed.

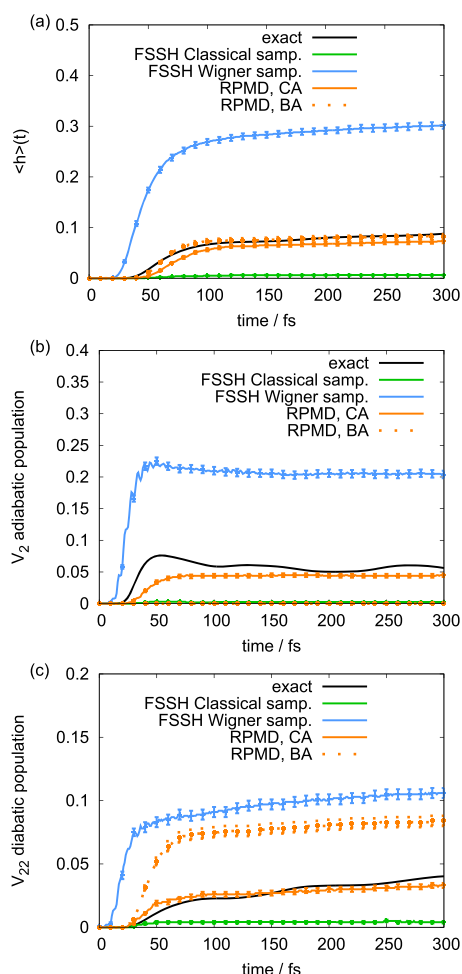


FIG. 5. Time-dependent side-expectation value (a), adiabatic (b), and diabatic populations (c) for an initial vibrational frequencies of 1500 cm^{-1} employing the weak coupling model. The initial excitation is to the lower state. Exact results are given in black, FSSH results with classical sampling (i.e., $n = 1$) in green, FSSH results with Wigner sampling in blue, and RPMD results employing the CA are given in solid orange lines and employing the BA in dashed orange lines.

V. CONCLUSION

We have presented a study of photodissociation employing RPMD with non-equilibrium initial conditions in combination with FSSH. RPSH performs well for all one-dimensional scenarios discussed. For cases where the crossing point is below the initial excitation, RPSH performs as well as FSSH, which can capture most of the exact quantum dynamics. For dynamics involving an energetically higher-lying crossing point, RPSH clearly outperforms standard FSSH with and without Wigner sampling. RPSH can reproduce the time-dependent dissociation probability well and also gives reasonable adiabatic and diabatic populations. Although only one-dimensional scenarios are discussed in this work, the generalization of the approach to any number of degrees of freedom is straightforward. Both RPMD and FSSH have been employed to treat

high-dimensional systems efficiently, and any equations presented here can be generalized in the same way.

The proposed approach can potentially be used to investigate excited-state proton transfer, where tunneling is important, e.g., in indole derivatives⁶² or phenol.^{54,63} In future work, it will be worth determining whether other nonadiabatic extensions of RPMD^{41–44,47,48,56} can outperform RPSH for the simulation of photodissociation dynamics or whether extensions developed for FSSH can improve the RPSH results. Furthermore, the influence of geometric phase effects on the dynamics described with RPMD merits some in-depth investigation.

REFERENCES

- O. P. Ernst, D. T. Lodowski, M. Elstner, P. Hegemann, L. S. Brown, and H. Kandori, *Chem. Rev.* **114**, 126 (2014).
- P. J. M. Johnson, A. Halpin, V. I. Prokhorenko, O. P. Ernst, and R. J. D. Miller, *Nat. Chem.* **7**, 980 (2015).
- C. Canuel, M. Mons, F. Piuze, B. Tardivel, I. Dimicoli, and M. Elhanine, *J. Chem. Phys.* **122**, 074316 (2005).
- M. Barbatti, A. J. A. Aquino, J. J. Szymczak, D. Nachtigallová, P. Hobza, and H. Lischka, *Proc. Natl. Acad. Sci. U. S. A.* **107**, 21453 (2010).
- K. Kleiner, D. Nachtigallová, and M. S. de Vries, *Int. Rev. Phys. Chem.* **32**, 308 (2013).
- M. A. Kochman, M. Pola, and R. J. D. Miller, *J. Phys. Chem. A* **120**, 6200 (2016).
- D. R. Yarkony, *J. Chem. Phys.* **100**, 18612 (1996).
- L. J. Butler, *Annu. Rev. Phys. Chem.* **49**, 125 (1998).
- J. C. Tully, *J. Chem. Phys.* **137**, 22A301 (2012).
- M. C. Persico and G. Granucci, *Theor. Chem. Acc.* **133**, 1526 (2014).
- I. Tavernelli, *Acc. Chem. Res.* **49**, 792 (2015).
- M. B. Smith and J. Michl, *Annu. Rev. Phys. Chem.* **64**, 361 (2013).
- H. Guo, P. Saalfrank, and T. Seideman, *Prog. Surf. Sci.* **62**, 239 (1999).
- S. Hammes-Schiffer, *Acc. Chem. Res.* **34**, 273 (2001).
- A. Soudackov and S. Hammes-Schiffer, *J. Chem. Phys.* **113**, 2385 (2000).
- R. I. Cukier and D. G. Nocera, *Annu. Rev. Phys. Chem.* **49**, 337 (1998).
- U. Manthe, H. Meyer, and L. S. Cederbaum, *J. Chem. Phys.* **97**, 3199 (1992).
- H.-D. Meyer, U. Manthe, and L. Cederbaum, *Chem. Phys. Lett.* **165**, 73 (1990).
- M. Beck, A. Jäckle, G. Worth, and H.-D. Meyer, *Phys. Rep.* **324**, 1 (2000).
- T. Westermann, R. Brodbeck, A. B. Rozhenko, W. Schoeller, and U. Manthe, *J. Chem. Phys.* **135**, 184102 (2011).
- M. Assmann, G. A. Worth, and L. González, *J. Chem. Phys.* **137**, 22A524 (2012).
- J. Schulze, M. F. Shibli, M. J. Al-Marri, and O. Kühn, *J. Chem. Phys.* **144**, 185101 (2016).
- J. Zheng, Y. Xie, S. Jiang, and Z. Lan, *J. Phys. Chem. C* **120**, 1375 (2016).
- C. Arnold, O. Vendrell, R. Welsch, and R. Santra, *Phys. Rev. Lett.* **120**, 123001 (2018).
- D. Mendiola-Tapia, E. Mangaud, T. Firmino, A. de la Lande, M. Desouter-Lecomte, H.-D. Meyer, and F. Gatti, *J. Phys. Chem. B* **122**, 126 (2018).
- J. C. Tully, *J. Chem. Phys.* **93**, 1061 (1990).
- P. J. Kuntz, *J. Chem. Phys.* **95**, 141 (1991).
- M. Barbatti, *Wiley Interdiscip. Rev.: Comput. Mol. Sci.* **1**, 620 (2011).
- M. Ben-Nun and T. J. Martinez, *Adv. Chem. Phys.* **121**, 439 (2002).
- I. R. Craig and D. E. Manolopoulos, *J. Chem. Phys.* **121**, 3368 (2004).
- I. R. Craig and D. E. Manolopoulos, *J. Chem. Phys.* **122**, 084106 (2005).
- I. R. Craig and D. E. Manolopoulos, *J. Chem. Phys.* **123**, 034102 (2005).
- B. J. Braams and D. E. Manolopoulos, *J. Chem. Phys.* **125**(12), 124105 (2006).
- T. F. Miller and D. E. Manolopoulos, *J. Chem. Phys.* **123**, 154504 (2005).
- S. Habershon, D. E. Manolopoulos, T. E. Markland, and T. Miller III, *Annu. Rev. Phys. Chem.* **64**, 387 (2013).
- R. Welsch, K. Song, Q. Shi, S. C. Althorpe, and T. F. Miller III, *J. Chem. Phys.* **145**, 204118 (2016).

- ³⁷T. J. H. Hele, M. J. Willatt, A. Muolo, and S. C. Althorpe, *J. Chem. Phys.* **142**, 134103 (2015).
- ³⁸T. J. H. Hele, M. J. Willatt, A. Muolo, and S. C. Althorpe, *J. Chem. Phys.* **142**, 191101 (2015).
- ³⁹S. Habershon, G. S. Fanourgakis, and D. E. Manolopoulos, *J. Chem. Phys.* **129**, 074501 (2008).
- ⁴⁰S. D. Ivanov, A. Witt, M. Shiga, and D. Marx, *J. Chem. Phys.* **132**, 031101 (2010).
- ⁴¹J. O. Richardson and M. Thoss, *J. Chem. Phys.* **139**, 031102 (2013).
- ⁴²N. Ananth, *J. Chem. Phys.* **139**, 124102 (2013).
- ⁴³J. R. Duke and N. Ananth, *Faraday Discuss.* **195**, 253 (2016).
- ⁴⁴S. N. Chowdhury and P. Huo, *J. Chem. Phys.* **147**, 214109 (2017).
- ⁴⁵P. Shushkov, R. Li, and J. C. Tully, *J. Chem. Phys.* **137**, 22A549 (2012).
- ⁴⁶F. A. Shakib and P. Huo, *J. Phys. Chem. Lett.* **8**, 3073 (2017).
- ⁴⁷X. Tao, P. Shushkov, and T. F. Miller, *J. Chem. Phys.* **148**, 102327 (2018).
- ⁴⁸A. R. Menzeleev, F. Bell, and T. F. Miller, *J. Chem. Phys.* **140**, 064103 (2014).
- ⁴⁹S. C. Althorpe, N. Ananth, G. Angulo, R. D. Astumian, V. Beniwal, J. Blumberger, P. G. Bolhuis, B. Ensing, D. R. Glowacki, S. Habershon, S. Hammes-Schiffer, T. J. H. Hele, N. Makri, D. E. Manolopoulos, L. K. McKemmish, T. F. Miller III, W. H. Miller, A. J. Mulholland, T. Nekipelova, E. Pollak, J. O. Richardson, M. Richter, P. Roy Chowdhury, D. Shalashilin, and R. Szabla, *Faraday Discuss.* **195**, 311 (2016).
- ⁵⁰L. Wang, A. Akimov, and O. V. Prezhdo, *J. Phys. Chem. Lett.* **7**, 2100 (2016).
- ⁵¹J. E. Subotnik, W. Ouyang, and B. R. Landry, *J. Chem. Phys.* **139**, 211101 (2013).
- ⁵²A. Jain, M. F. Herman, W. Ouyang, and J. E. Subotnik, *J. Chem. Phys.* **143**, 134106 (2015).
- ⁵³A. Jain and J. E. Subotnik, *J. Chem. Phys.* **143**, 134107 (2015).
- ⁵⁴C. Xie, J. Ma, X. Zhu, D. R. Yarkony, D. Xie, and H. Guo, *J. Am. Chem. Soc.* **138**, 7828 (2016).
- ⁵⁵R. Kubo, *J. Phys. Soc. Jpn.* **12**, 570 (1957).
- ⁵⁶J. T. Hele, Master's thesis, University of Oxford, 2011.
- ⁵⁷J. C. Tully, *Faraday Discuss.* **110**, 407 (1998).
- ⁵⁸S. Bazzi, R. Welsch, O. Vendrell, and R. Santra, *J. Phys. Chem. A* **122**, 1004 (2018).
- ⁵⁹M. K. Ganesa Subramanian, R. Santra, and R. Welsch, *Phys. Rev. A* **98**, 063421 (2018).
- ⁶⁰T. F. Miller and D. E. Manolopoulos, *J. Chem. Phys.* **122**, 184503 (2005).
- ⁶¹G. A. Worth, M. H. Beck, A. Jäckle, O. Vendrell, and H.-D. Meyer, The MCTDH Package, 2015.
- ⁶²R. Welsch, E. Driscoll, J. M. Dawlaty, and T. F. Miller III, *J. Phys. Chem. Lett.* **7**, 3616 (2016).
- ⁶³X. Zhu and D. R. Yarkony, *J. Chem. Phys.* **144**, 024105 (2016).